Estimation of PP- wave ray impedance from elastic impedance

Feng Zhang, and Xiangyang Li, Edinburgh Anisotropy Project, British Geological Survey, UK
Yanghua Wang, Centre for Reservoir Geophysics, Imperial College London, UK

Summary
Theoretical evaluation of elastic impedance (EI) and ray impedance (RI) reveals that RI has a more reliable dimension and is less sensitive to errors than EI. In this paper, a new measurement ($\tilde{\text{RI}}$) is proposed to estimate ray impedance from the elastic impedance derived by existing techniques. The recovered $\tilde{\text{RI}}$ is expressed in the form of a normalization of the elastic impedance (EI), and it has the same dimension and interpretation capability as RI. Tests of these three measurements are performed on the log data of three different types of reservoir: a typical Class III marine gas sand, a Class I tight gas-sand and an oil-bearing sand in thin sand-mud inter-bedded layers. We show that RI is capable of characterizing all three types of reservoir. In particular, it appears to be more applicable than EI for characterizing tight gas sands. The cross-plots of EI against acoustic impedance (AI) show good characterization for gas sand, but approximately linear trends are found for all three cases. $\tilde{\text{RI}}$, estimated from EI, has a comparable dimension to the acoustic impedance (AI), and retains the interpretation ability of the original RI.

Introduction
The reflection coefficient is determined by the elastic parameters of the subsurface medium, and varies with the angle of incidence (ray parameter). The reflection coefficient can be described by the Zoeppritz equations, which are derived from the wave equations. The reflectivity at the *i*th interface can be expressed in a recursive form of elastic impedance above and below the interface,

$$R_{ppi}(\theta_i) = \frac{EI_{i+1} - EI_i}{EI_{i+1} + EI_i} \approx \frac{1}{2} \ln \frac{EI_{i+1}}{EI_i}. \quad (1)$$

As a generalization of AI, the elastic impedance (EI) is defined as (Connolly, 1999)

$$EI_i(\theta_i) = \alpha_i \rho_i (\alpha_i^{\tan^2\theta_i} \beta_i^{-8K\sin^2\theta_i} \rho_i^{4K\sin^2\theta_i}), \quad (2)$$

where α_i, β_i and ρ_i is P-wave velocity, S-wave velocity and density of the medium layer; θ_i is the angle of incidence; the parameter $K = \beta^2/\alpha^2$ is assumed to be constant, where α and β are the average velocities of two adjacent media. Besides the P-wave reflection, elastic impedance also represents the reflection of the converted shear wave. EI inversion has been applied widely in hydrocarbon prediction because, given an angle of incidence, EI inversion can be performed on prestack seismic data, similarly to AI inversion.

The derivation of EI is based on two well-known assumptions: (1) Angles of incidence are constant; and (2) the parameter $K = \beta^2/\alpha^2$ is constant. The first assumption does not follow Snell's law, and EI only represents the physical property of subsurface media within a limited interval. Besides, EI is very sensitive to non-optimal values of *K*, because huge differences between these EI estimates can be found. An interpretation limitation of EI is that its dimension varies dramatically with the angle of incidence. Although a normalized form of EI is proposed in Whitcombe (2002), where reference measurements for the interval of interest are used, it is sensitive to not only the non-optimal values K but also the normalization reference measurements (Zhang, 2010).

The ray impedance (RI) is defined along the ray path (Wang, 2003): at the *i*th interface:

$$RI_i(p(\theta_i)) = \frac{\alpha_i \rho_i}{\sqrt{1-\alpha_i^2 p^2}} (1-\beta_i^2 p^2)^{2(r+2)} = \frac{\alpha_i \rho_i}{\cos\theta_i} \left(1 - \frac{\beta_i^2}{\alpha_i^2} \sin^2\theta_i\right)^2 \quad (3)$$

where $p = \sin\theta_i / \alpha_i$ is the ray parameter or horizontal slowness, and $r = (\Delta\rho/\rho)/(\Delta\beta/\beta)$ is assumed to be constant. The derivation of ray impedance is based on the linearized approximation of reflection coefficients in the ray parameter domain (Wang, 1999)

$$R_{ppi}(p) = R_f - 2\frac{\Delta\mu}{\rho} p^2, \text{ and} \quad (4)$$

$$R_f = (\rho_{i+1} q_{\alpha i} - \rho_i q_{\alpha(i+1)}) / (\rho_{i+1} q_{\alpha i} + \rho_i q_{\alpha(i+1)}), \quad (5)$$

where q_α is the P-wave vertical slowness; $\Delta\mu = \rho_{i+1}\beta_{i+1}^2 - \rho_i\beta_i^2$ is the contrast in shear modulus. Since the ray parameter is constant at different depth, RI can be used to describe subsurface media over an arbitrary depth interval. In this sense, ray impedance is the generalization of the angle-dependent elastic impedance. Although the parameter $r = (\Delta\rho/\rho)/(\Delta\beta/\beta)$ is assumed to be constant, RI is insensitive to the non-optimal values of *r*; besides, RI for larger ray parameters generally gives better discrimination of hydrocarbon reservoir from surrounding rocks, and it has little dimensionality difference from RI with smaller ray parameters or AI (Zhang, 2010).

Transformation from EI to RI
Although RI shows advantages in interpretation, it is still a new measurement to the industry compared with EI. Geophysicists have been used to generate seismic angle gathers using developed techniques. EI is then inverted from the seismic data within a range of incident angles.

Therefore, besides quantitative comparison of EI with RI, it is meaningful to build a direct link between these two valuable tools.

		Vp (km/s)	Vs (km/s)	Density (km/s)*(g/cc)
Model 1	Upper	4.316	2.437	2.65
	Lower	5.3357	3.0	2.48
Model 2	Upper	2.886	1.016	2.271
	Lower	2.548	1.366	2.031
Model 3	Upper	4.054	1.995	2.4
	Lower	4.777	2.817	2.269

Table 1. Parameters of three single-interface models.

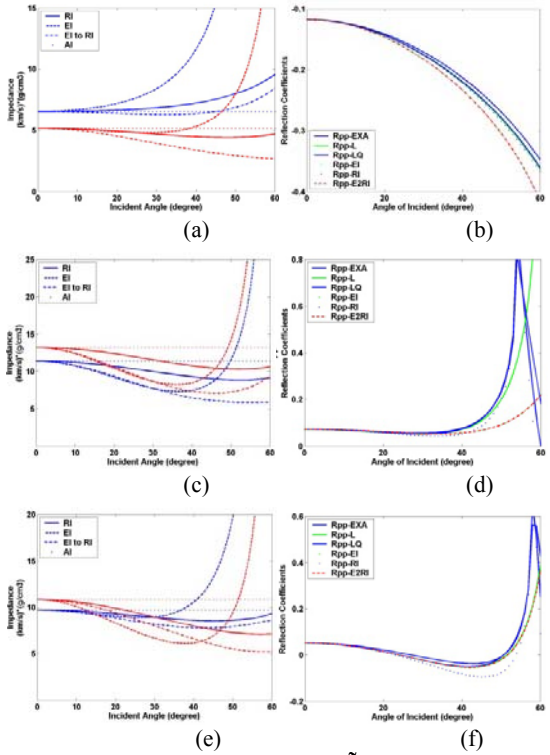

Figure 1. Comparison of RI, EI and $\tilde{R}I$ for the three models in Table 1: (a) Model 1, (c) Model 2 and (e) Model 3. AVO curves for the three models are shown in (b), (d) and (f).

In order to retain their own physical meanings, this analysis is performed in the angle domain using the single interface models in Table 1. An analytic formula is proposed to estimate the ray impedance from the elastic impedance. This estimated ray impedance is denoted as $\tilde{R}I$. $\tilde{R}I$ is a combination of the above two attributes (EI and RI), and can be expressed in the form of a normalization of EI:

$$\tilde{RI}_i(p(\theta_i)) \approx EI_i \frac{\alpha^{\tan^2\theta}\eta_i}{\cos\theta_i}, \qquad (6)$$

where α is the average velocity of the section of interest, $\eta_i = \cos^{4(r+2)}\varphi_i\beta_i^{4\tan^2\varphi(r+2)}$. $\tilde{R}I$ represents the elastic property of a medium within a certain depth/time interval. It has the same physical property as EI, but has similar interpretation capability to RI.

Figure 1 shows the comparisons of these measurements for the models in Table 1. In Figures 1a, 1c and 1e, solid curves are RIs, dashed curves represent EIs and $\tilde{R}I$s. AIs are also plotted as straight dotted lines. Shale and sand layers are blue and red, respectively. AVO curves for the three models are shown in (b), (d) and (f). The black curves represent reflection coefficients from the exact Zeoppritz equation. Solid green and blue curves represent the linearized approximations from which EI and RI are derived (equations 1 and 5); the dotted green and blue lines respectively show the approximations calculated from EI and RI. The dashed red curve is the reflectivity derived from $\tilde{R}I$.

After the transformation from EI curves using expression (6), $\tilde{R}I$ curves have comparable dimension to AI, and similar variation as RI curves with increasing incident angle. Figure 2 also compares the reflectivity derived from EI, RI and $\tilde{R}I$. We can see that the reflectivity of $\tilde{R}I$ (red dashed curves) agrees well with that of EI, even at very wide angles of incidence.

Real data application

We use real log data in three cases (Figure 2), representing different types of reservoir, to evaluate the interpretation capability of elastic impedance and ray impedance, and test the feasibility of estimated $\tilde{R}I$. These cases are: case 1, a typical Class III marine gas sand; case 2, a Class I tight gas-sand; and case 3, an oil-bearing sand of thin sand-mud inter-bedded layers. Cross-plots of EI, RI and $\tilde{R}I$ at far offset versus AI are plotted to discriminate the hydro-carbon bearing sands from shales. Then $\tilde{R}I$ is estimated on the real inverted EI section for the tight sand gas reservoir, and is compared with the inverted RI.

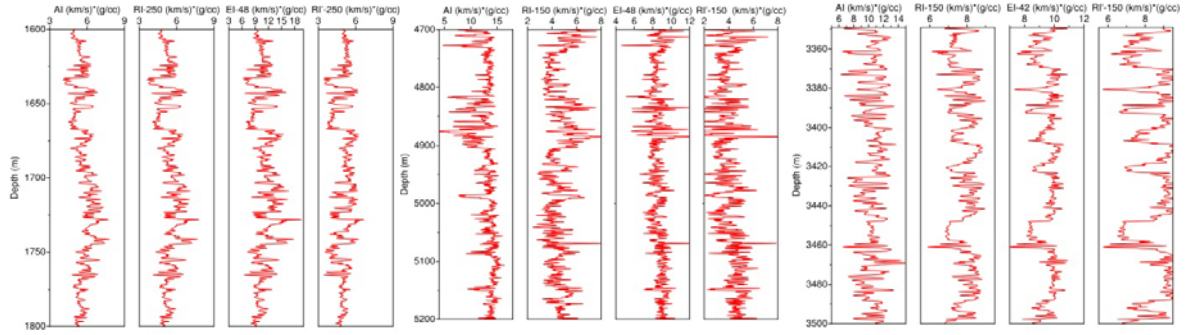

(a) (b) (c)

Figure 2. Comparison of AI with RI, EI and R̃I for the wells in (a) case 1, (b) case 2 and (c) case 3.

Case 1: This reservoir formation is a traditional Class III gas sand, buried in clastic deep-sea turbidites. It has high porosity (>25%) and permeability. Figure 3 compares the cross-plots of the forms of elastic impedance (EI, RI and R̃I) versus acoustic impedance. The gamma ray log is used for lithology characterization, while the porosity log is used to indicate fluid. Cross-plots of RI (250ms/km*)* and EI (48^o) give a similar characterization of rocks (Figure 3a-3b). Both of them show good discrimination of sand (green) from shale (purple). EI has the value (6000-17000m/s*g/cc) as twice as that of RI (2750-8000m/s*g/cc); R̃I (3000-7000m/s*g/cc) has a similar dimension to RI and AI (3500-7750m/s*g/cc). This transformation does not compromise the interpretation ability of EI: a clear view of sand can also be found in the cross-plot of R̃I (Figure 3c). Fluid analysis (Figure 3d – 3f) shows that those sands with higher porosity (purple) have a lower impedance value (2500-4500m/s*g/cc for RI).

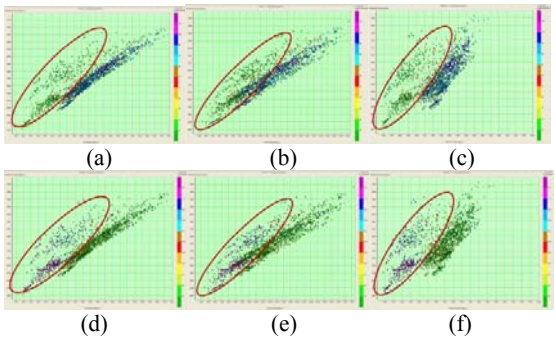

(a) (b) (c)

(d) (e) (f)

Figure 3. (a) - (c) Cross-plots of RI (250ms/km), EI (48°) and R̃I (250ms/km), respectively for the reservoir in case 1: colour key represents gamma ray and porosity. (d) – (f) Same as (a) – (c), colour key represents porosity. Sands are marked with red circles.

Case 2: This Class I gas sand is an unconventional resource - tight clastic sediments with extremely low porosity (average 2.9%) and permeability (average 3.9mD). In this case, sands are shaly and are difficult to discriminate from surrounding shales even using the far-offset elastic impedance: in Figure 4b and 4e, EI(48^o) sands are mixed with the signature of shale. Corresponding ray impedance (150ms/km) shows a better interpretation of the reservoir (Figure 4a and 4d). This ability is also retained by the estimation of R̃I from elastic impedance (Figure 4c and 4f). In Figure 4d – 4f, tight sand shows lower porosity (2% in green) than surrounding shales (purple).

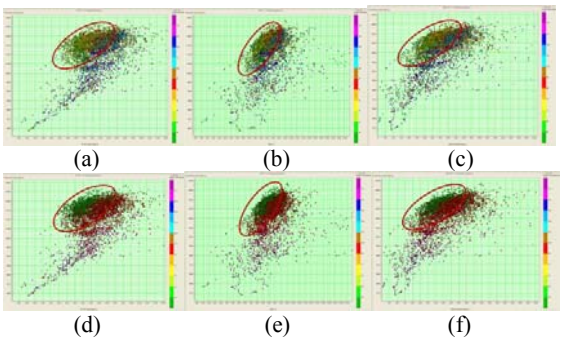

(a) (b) (c)

(d) (e) (f)

Figure 4. (a) - (c) Cross-plots of AI with RI (150ms/km), EI (45^o) and R̃I (150ms/km) for case 2, colour key represents gamma ray. (d) – (f) Same as (a) – (c), colour key represents porosity. Sands are marked with red circles.

Case 3: The final analysis is performed on a reservoir of multiple thin oil-bearing sand layers (inter-bedded sand-mud layers). Porosity and permeability are also low, from 10.4% to 13.9%, and from 14.7 to 0.06mD, respectively. In this case, although good discrimination is also found in the cross-plot of EI (Figure 5b), a clearer view of sand (green) seems to be found in the RI and R̃I sections (Figure 5a and 5c). As in case 1, oil sands with higher porosity (14% in blue) have a lower impedance value.

As shown in Figure 6, EI(48°) and RI(150ms/km) sections are inverted using the seismic data for the tight sand reservoir. Corresponding well logs and the related horizon are also plotted on the inverted sections in Figure 6. Compared with inverted EI, sand bodies in RI section show clearer contrast (higher impedance regions at well location) and therefore can be identified. This property can also be recovered from the estimated $\tilde{R}I$ using equation (6). Regions with higher impedance values are highlighted during this transformation. Besides, the values of impedance are compressed within the range between 2 to 10 (km/s)*(g/cc).

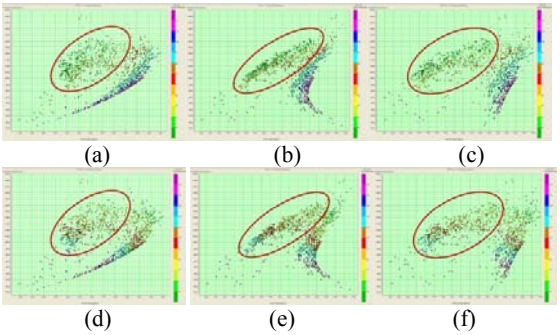

Figure 5. (a) – (c) Cross-plots of AI with RI (150ms/km), EI (42°) and $\tilde{R}I$ for case 3, colour key represents gamma ray and porosity. Same as (a) – (c), colour key represents porosity. Sands are marked with red circles.

Conclusions

Due to the assumption of constant angle of incidence, elastic impedance can only represent physical properties for media within a limited interval. In reservoir characterization, EI needs to be used carefully, because of its unstable dimensionality and non-optimal values of *K*. Even though, EI shows good discrimination of hydro-carbon reservoirs from surrounding rocks for a typical Class III gas sand. Ray impedance can be used to describe continuous media within an arbitrary interval. Because of the reliable dimensionality and non-sensitivity to errors, ray impedance is more applicable than elastic impedance for reservoir characterization. We propose a new measurement $\tilde{R}I$ that is estimated from EI, which has the similar interpretation capability and corresponding dimension as RI. In log data analysis for three types of reservoirs, cross-plots of elastic impedance against acoustic impedance represent nearly linear fitting because of the constant background *K*. Cross-plots of RI and AI show a similar interpretation as EI for the typical Class III gas sand, but show better discrimination of hydrocarbon-bearing sand from shale for the other two cases. $\tilde{R}I$ estimated from EI has a comparable dimension to the acoustic impedance, and maintains the interpretation ability of the original RI. The inverted result is improved using $\tilde{R}I$, as sand layers can then be clearly identified in the $\tilde{R}I$ section as the RI section.

Acknowledgement

We are grateful to the sponsors of the Centre for Reservoir Geophysics, Imperial College London, and the Edinburgh Anisotropy Project at the British Geological Survey, Edinburgh, for supporting this research.

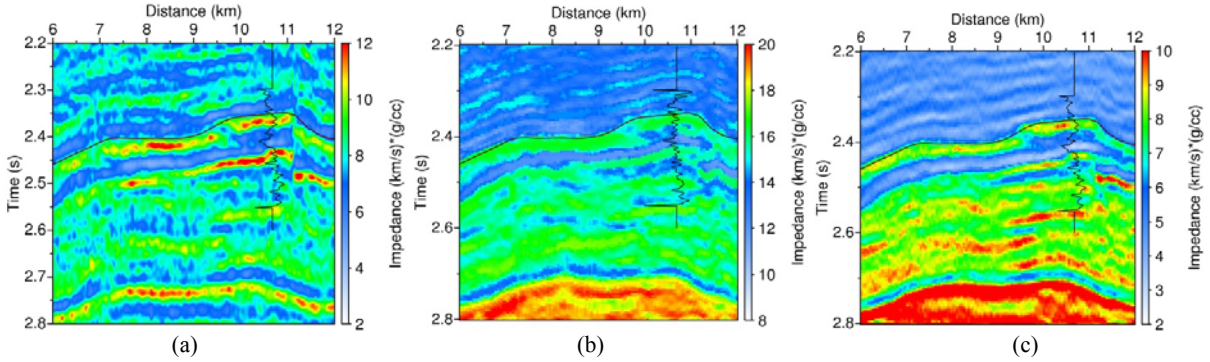

Figure 6. Inverted section of RI (150ms/km), EI (48°) and $\tilde{R}I$ (150ms/km) for the reservoir in case 2. Gas-sand is represented by high impedance value. Corresponding well logs are plotted.